# Variational Constraints for Data Assimilation in ALADIN-NH Dynamics

Carlos Geijo, Pau Escribà, Spanish Meteorological Agency (AEMET)

## 1 Introduction

Balances among analysed meteorological variables in the data assimilation process can be effectively introduced by means of the well-known method of variational constraints (VC) [1], [2], [3]. In the case of the ALADIN-NH dynamics, its semi-implicit linear system for the non-hydrostatic fully compressible Euler equations (SI) appears as a convenient way of giving a precise definition to these constraints. This approach is non-statistical and in principle flow-dependent. Non-isotropic and non-homogeneous aspects in the analysis increments cannot however be fully introduced by these constraints because SI deals only with rotation invariants and the base-state used in its formulation is one at rest and on a flat orography. The spatial structure in the analysis will then come only from the spatial structure of the observation increments forcing. In this respect, the situation is similar to the current ALADIN 3D-Var algorithm [4], although now these restrictions stem not from assumptions on the statistical properties of the model error fields, but from the definition of the SI itself. A new interesting feature of this method is the integration in the analysis algorithm of the vertical velocity field, which clearly must be important in convection permitting NWP. Another main point is that SI is a time-step forward operator, and this property gives to this algorithm a nudging-like functionality making it well suited for DA continuous-in-time, also an indispensable feature for NWP of intrinsically short-time predictability weather.

SI can be solved using Greens functions (GF) [5]. Because of the assumptions behind its formulation, SI can be reduced to an ODE boundary value problem whose GF is easy to calculate and permits the solution to be found by quadratures. This GF algorithm has the appealing feature of doing the mathematics very transparent (in particular the treatment of upper and lower boundary conditions), avoids staggering along the vertical and also goes around the problem of the algebraic constraints among discrete local and non-local operators. In this work this GF method is pursued further and it is shown that the analysis with variational constraints can be found by a similar numerical algorithm, although now involving GFs for higher order operators.

VC has been tested in three different contexts. First it is applied to increments obtained from the alignment of radial wind HARMONIE-AROME fields with Doppler radar pseudo-images employing a position error correction algorithm known as Field Alignment (FA) [6]. This FA is a fully flow-dependent algorithm, but it introduces imbalances which have a detrimental impact in subsequent forecasts. VC can effectively reduce these imbalances. The VC method was conceived with this first application in mind, in the scope of the development of new NWP tools for Now-Casting (NWP-NWC). Second, it is applied to LETKF analysis [7] generated from a small ensemble. The lack of overlap in observations used by the analysis in neighbouring points causes discontinuities in the analysed fields that VC can filter according to the dynamics described by SI. Third, a comparison between VC and the statistical balances implemented in the current 3D-Var algorithm [8] was conducted in order to get a first estimate of the impact of this new approach, in particular of including in the initialization the vertical wind.

## 2 Variational Constraints for ALADIN-NH Dynamics

In the spirit of the GF algorithm, we will consider the minimization of a functional J on functions of a given degree of smoothness in the vertical coordinate $\xi$ and see whether or not the problem can be solved in this framework. Let as usual J consist of an observation forcing term and a constraint, weighted by $w_o$ and $w_c$ respectively:

$$2J(x^k) = \int_o^{\xi} w_o^k \left\| x^k - x_o^k \right\|^2 + w_c^k \left\| Mx^k - x_\bullet^k \right\|^2 \qquad Eq\ 2.1$$

where the upper index k indicates that the problem is stated in wavenumber space. The module bars $\|\cdot\|$ come in because the x's are complex numbers. M stands here for the SI system, it encodes the set of constraints and is a real operator, what makes the introduction of these complex module bars unnecessary after all (M does not mix real and imaginary parts of $x_k$). This conclusion is apparent from simple inspection of Eq2.1, but in case of non correspondence between model and obs spaces (i.e. when an obs operator is necessary) it takes some algebra to conclude that it is also possible to dispense with the complex module bar notation (see [9]). The symbol "●" is introduced to keep in mind a subtle difference with the similarly looking 3D-Var cost function, where one would write $x_b$ instead of $x_\bullet$. M is a time-step advancing operator, $x_\bullet$ and $x_b$ correspond then to model states at different times (differing by one time step). In principle the weights $w_o$ and/or $w_c$ could vary along the $\xi$ coordinate, but this would complicate the calculation of the GF used by the numerical method that it is wanted to show in this paper. Therefore it is not considered here. Also these weights could take different values for different wavenumbers, this does not really complicate things, but at this stage it is considered a refinement of secondary importance. Therefore the weights $w_o$ and $w_c$ are just two real numbers and their ratio ($w = w_o/w_c$) is the only free parameter in the scheme.

One first obstacle in the calculation proposed in Eq2.1, is the determination of $x_o^k$. The problem arises because the observation fields will unavoidably be irregularly distributed in space and display void areas. To go around this difficulty let us restrict to an incremental formulation of the problem, that is, search for a solution in the vicinity of the background $x_b$

$$x^k = x_b^k + \Delta x^k \quad ; \quad x^k - x_o^k = -d^k + \Delta x^k \quad ; \quad d^k = x_o^k - x_b^k \quad ; \quad Mx^k - x_\bullet^k = M\Delta x^k \qquad Eq\ 2.2$$

the last equation follows because the background is, of course, balanced. The difference field d does not have holes and it can readily be DFT transformed back and forth. Dropping the k upper index, Eq2.1 becomes:

$$2J(\Delta x) = \int_o^{\xi} w \left(\Delta x - d\right)^2 + \left(M\ \Delta x\right)^2 \qquad Eq2.3$$

The condition that the increments $\Delta x$ are balanced is seen to translate into the condition that they belong to the kernel of M, but in this weak-constraint approach, this condition will only be approximately satisfied. Take now functional variations of J ($\delta J$) and disregard the boundary terms that results in the calculation. This can be done because we leave the values of $\Delta x$ and $\partial\Delta x$ at the top and bottom boundaries out of the data assimilation problem, they will not be considered as control variables, that is, take $\delta\Delta x = \delta(\partial\Delta x) = 0$ on the boundaries (which does not mean that $\Delta x = \partial\Delta x = 0$ there necessarily, they can be given other values if non-homogeneous BC are specified, see below). Equating to zero the first variation gives

$$M^+M\ \Delta x + w\,\Delta x = w\,d \qquad w \equiv \frac{w_o}{w_c} \quad Eq\ 2.4$$

where $M^+$ is the adjoint of M with regard to the inner product used in the definition of J. It turns out that this problem can be reduced to an ODE boundary value problem which can be solved with homogeneous or non-homogeneous boundary conditions (BC) on $\Delta x$ by means of the corresponding GF (see [9] for a detailed derivation of this result).

### 2.1 Formulation of the Balances

The SI system consists of set of linear equations with local and non-local vertical operators. The non-local operators arise because it is written in a mass-based vertical coordinate [12]. By decoupling the different horizontal wavenumbers, it becomes a very efficient time-stepping algorithm. Different formulations of it have been considered depending on the choice of prognostics. These formulations are all consistent within the linear approximation of the so-called "state equation" and geopotential equation (i.e. they can be transformed into each other by using Eq2.6 below). It is very convenient to go to non-dimensional variables by using the scales for T, $\pi_s$ and the time-step $\Delta t$, and also to use a "depth $\xi$" coordinate (runs downwards from 0 to $\underline{\xi}$, see [5],[9] for all details). The choice in this work is the GEO-GW formulation, which after time discretization and before vertical discretization reads

$$D - K^2\left(T + (\partial+1)\Psi\right) = D^{\bullet} \qquad K^2 = (kH)^2\,\omega_b^2 \quad \omega_b^2 = \frac{g\,\Delta t^2}{H} = \frac{g^2\,\Delta t^2}{RT^*} \quad ; \quad D = D'\,\Delta t$$

$$gw - \omega_e^2\left((\partial+1)T + (\partial+1)\partial\Psi\right) = gw^{\bullet} \qquad \omega_e^2 = \frac{g^2\,\Delta t^2}{RT_e^*} \qquad gw = gw'\,\Delta t \Big/ RT_e^*$$

$$T + \frac{R}{c_v}\left(D - \chi\,\partial gw\right) = T^{\bullet} \qquad T = T' \Big/ T^* \quad \chi = \frac{T_e^*}{T^*} \qquad Eq\ 2.5$$

$$\pi_s + N[D] = \pi_s^{\bullet} \qquad \pi_S = \pi_S' \Big/ \pi_S^*$$

$$\Psi - \chi\,gw + S[D] = \Psi^{\bullet} \qquad \Psi = (\Phi_S + \Phi') \Big/ RT^* + \pi' \Big/ \pi^*$$

The time step $\Delta t$ includes numerical factors that depend on the choice of the time discretization scheme. The primed variables denote the perturbation (i.e. departure from base-state). For the wind (D and gw) they actually are the full variable as the base-state is at rest. The differentiation and integration operators are $\partial$, S[ ] and N [ ]=S [ ] ($\xi=\underline{\xi}$ ). In this notation, the state equation and geopotential equation read ([9])

$$PD = \partial\Psi + T = \partial\Phi + \partial\pi + T\,; \quad \Phi(\xi) - \Phi(\underline{\xi}) = -G[\partial\Phi] = -G[PD] + G[T] + \pi_s - \pi \quad Eq2.6$$

With PD the pressure departure ( PD= ln(p/π), p=total pressure, π="hydrostatic pressure" ) and G[ ] another integration operator. In Eq2.5 two different T scales are employed, and their ratio is denoted as $\chi$. This duplicity of T scales is considered here because it has been reported that it has impact on the stability of the vertical finite differences (FD) numeric scheme [10]. In fact, $\chi$=1/5 in the FD solver implemented in the HARMONIE-AROME system and used for this work.

As mentioned in the introduction, Eq2.5 can be reduced to an ODE boundary value problem. A vertical discretization based on splines is used for this porpoise [5]

$$\left(-\lambda + \partial(\partial+1)\right)[\chi\,gw] = -\frac{\left(1+K^2\gamma\right)}{\omega_e^2\chi\,\gamma}\chi\,gw^{\bullet} + \left(\frac{R}{c_p} + \partial\right)D^{\bullet} - \frac{1}{\gamma}\left(\partial + 1 + K^2\right)T^{\bullet} - \left(\frac{1}{\gamma}\partial - \frac{R}{c_p}K^2\right)(\partial+1)\,\Psi^{\bullet}$$

$$\left(1+K^2\gamma\right)D - K^2\left(1+\gamma\partial\right)\chi\,gw = D^{\bullet} + K^2\left((\partial+1)\Psi^{\bullet} + T^{\bullet}\right)$$

$$T + \frac{R}{c_v}\left(D - \chi\,\partial gw\right) = T^{\bullet} \qquad \lambda = \frac{1 + K^2\,\gamma\,(1 + \omega_e^2\,\chi\,R/c_p)}{\omega_e^2\,\chi\,\gamma} \quad Eq2.7$$

$$\pi_S + N[D] = \pi_S^{\bullet}$$

$$\Psi - \chi\,gw + S[D] = \Psi^{\bullet} \qquad (*) \quad \omega_e^2\chi = \omega_b^2$$

This re-arrangement of the equations can be referred to as M[$x_b$ + $\Delta$x] in Eq2.3 notation. It needs to be complemented with BC on $\Delta$gw (or perhaps on $\partial\Delta$gw or both) at $\xi$=0 and $\xi=\underline{\xi}$. It is interesting to see that, because of the relation indicated in Eq2.7 as (*), the double T-scaling has no effect on the free-mode unbounded spectrum of M, obtained by setting M[x]=0 with periodic BC (e.g. gw(0)=gw($\underline{\xi}$)=0).

## 2.2 A Numerical Solution to VC using GF

Eq2.7 shows a set of five constraints that are implied in SI. Of the five prognostics (gw, D ,T, $\pi_s$, Ψ), the last one Ψ will hardly ever be accessible to observations. As the equation of state Eq2.6 shows, it is closely connected to PD, a variable that is defined by a rather arbitrary partition of the total true pressure p. As in addition to this it also happens that leaving this Ψ-constraint out of the common treatment of the other four greatly simplifies the mathematics of the problem, we will consider just the set of the first four (vertical velocity, horizontal divergence, T-compressibility and surface pressure tendency). With $\chi$=1 we can write for M and its adjoint $M^+$

$$M=\begin{bmatrix} L & 0 & 0 & 0 \\ -K^2(1+\gamma\,\partial) & (1+K^2\,\gamma) & 0 & 0 \\ -\beta\,\partial & \beta & 1 & 0 \\ 0 & N[\ ] & 0 & 1 \end{bmatrix} \quad M^+=\begin{bmatrix} L^+ & -K^2(1-\gamma\,\partial) & \beta\,\partial & 0 \\ 0 & (1+K^2\,\gamma) & \beta & N^+[\ ] \\ 0 & 0 & 1 & 0 \\ 0 & 0 & 0 & 1 \end{bmatrix} \quad Eq2.8$$

where $\beta=R/c_v$ , $\gamma=c_p/c_v$ , $K^2$ defined in Eq2.5 and

$$S[X]=e^{-\xi}\int_0^{\xi} e^{z}\,X \qquad S^+[X]=e^{\xi}\int_{\xi}^{\bar{\xi}} e^{-z}\,X \qquad N[X]=e^{-\bar{\xi}}\int_0^{\bar{\xi}} e^{z}\,X \qquad N^+[X]=e^{\xi-\bar{\xi}}\int_0^{\bar{\xi}} X$$

$$L[X]=(\partial^2+\partial-\lambda)X \qquad L^+[X]=(\partial^2-\partial-\lambda)X+BT_L \qquad \partial[X]=\partial X \quad \partial^+[X]=-\partial X+BT_\partial \quad Eq\ 2.9$$

with BT meaning “boundary term”. As explained above, the BT vanish because the BC are not considered control variables. The adjoints of the integral operators can be found by application of the defining property of adjoints (i.e. $<O^+X,Y> = <X,OY>$ ). At difference to the local operators L or $\partial$, these non-local operators do not give boundary terms (see [9] for all details).

With these ingredients, it happens that Eq2.4 leads to another ODE boundary value problem as it happened for M (Eq2.7). However, now the operator involved is of 4th order instead of 2nd order

$$\hat{O}_{\xi}[\,\Delta gw\,]= \quad F^o_{gw}(\xi) \quad + \quad F^o_D(\xi) \quad + \quad F^o_T(\xi) \quad + \quad F^o_{\pi_s}(\xi)\left(d_{\pi_s}+N[\Delta D]\right) \quad Eq2.10$$

The F°´s on the r.h.s denote functions of the differences between observations and background for the corresponding variable ($d = x_o - x_b$ ), which are functions of ξ . They also depend on the relative weights “w” between obs forcing terms and constraints. It is possible to keep the possibility of these weights being different for each constraint

$$F^o_{gw}(\xi)=w_{gw}\,d_{gw}(\xi) \quad ; \quad F^o_D(\xi)=\frac{1}{X}\left(F_k\,K^2(1-\gamma\,\partial)-\beta^2\,\omega_T\,\partial\right)[\,w_D\,d_D(\xi)\,] \qquad Eq2.11$$

$$F^o_T(\xi)=-\frac{\beta}{X}\left((F_k+w_D)\,\partial+F_k\,K^2\right)[\,\omega_T\,d_T(\xi)\,] \quad ; \quad F_k=1+\gamma K^2 \quad X=F_k^2+w_D+\omega_T\beta^2$$

$$F^o_{\pi_s}(\xi)=\frac{1}{X}\left(F_kK^2\beta+\omega_T\beta^2\right)\omega_\pi e^{\xi-\bar{\xi}} \qquad ; \quad \omega_i=\frac{w_i}{1+w_i} \quad i=gw,D,T,\pi_s$$

and the 4th operator for which we have to find the GF is ( λ is defined in Eq2.7 )

$$\hat{O}_{\xi} = \partial^4 - a\,\partial^2 + b \quad ; a = (2\lambda+1) + \frac{1}{X}\left(K^4\gamma^2 w_D + (1+w_D)\omega_T\beta^2\right) \quad ; b = w_{gw} + \lambda^2 + \frac{1}{X}\left(\omega_T\beta^2 + w_D\right)K^4 \qquad Eq2.12$$

and as boundary conditions for the analysis increments Δgw we choose (non-homogeneous BC can also be incorporated if wanted).

$$\Delta gw(0) = \Delta gw(\underline{\xi}) = \partial\Delta gw(0) = \partial\Delta gw(\underline{\xi}) = 0 \quad ; \quad Eq2.13$$

The last term on the r.h.s of Eq2.10 is the obs forcing due to surface pressure increments. It shows up as proportional to a quantity N[ΔD] that at the time of performing quadratures with $O_{\xi}^{-1}$ (i.e. GF) is still unknown. However, this unknown is not a function of ξ, is just a number, and the quadratures can be carried out without more trouble giving us back a solution parametrized by this quantity N[ΔD].

$$\Delta gw(\xi) = P(\xi) + Q(\xi)\left(F_{\pi_s} + N[\Delta D]\right); \quad P(\xi) = \sum_{i=1}^{3}\int_0^{\bar{\xi}} \hat{O}^{-1}(\xi,z)\,F_i^o(z) \quad , Q(\xi) = \int_0^{\bar{\xi}} \hat{O}^{-1}(\xi,z)\,F_{\pi_s}^o(z) \quad Eq2.14$$

This remaining d.o.f is fixed by performing the calculation N[ ] on the second constraint with the solution found as in Eq2.14. How to do this accurately is also shown in [9]. It is then straightforward to substitute back in the rest of the constraints and so obtain finally the complete VC solution.

Eq2.11 shows that the analysed vertical velocity field (and therefore all the other analysed fields) is given by the ob - fg increments low-pass and high-pass filtered ($K^2$ dependency of the coefficients). These filters are not defined at will (aside from the values arbitrarily given to the weights "w"), but determined by SI. The vertical structure of the ob - fg increments ($\partial$ dependency of the coefficients) also enters in the determination of the analysis. Horizontal and vertical structure of the analysis are then intertwined as dictated by SI.

The determination of the GF for the problem Eq2.12, Eq2.13 is one key element in this scheme. The high amount of symmetry in the problem (only even powers of $\partial$, constant coefficients and hermiticity) makes it an accessible one, and makes also the whole scheme practical. The solution is worked out in [9]. Some examples of the GF kernels are shown in figure 1.

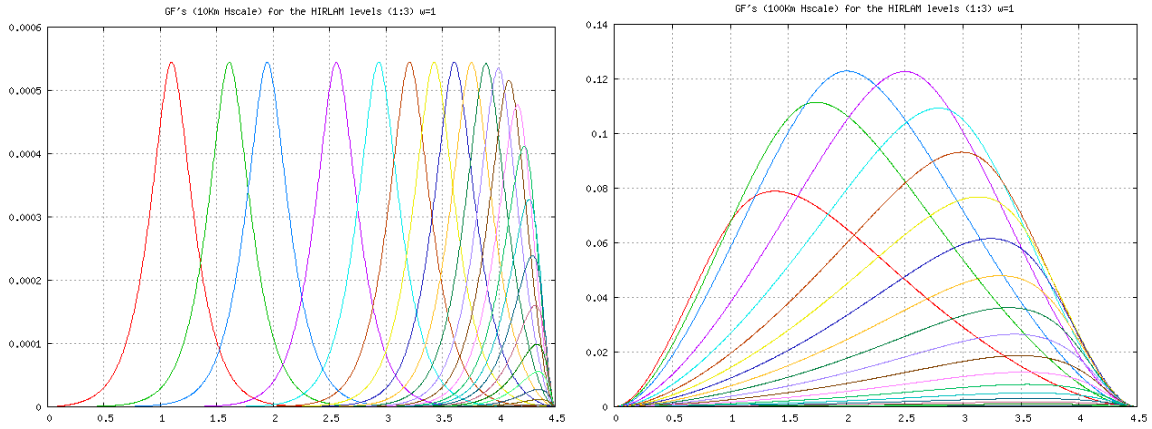


***Figure 1*** *Aspect of the GF kernels for the problem Eq2.12, Eq2.13 corresponding to horizontal scales of 10 km (left) and 100km (right) with w=1 and HIRLAM 65-levels (only 1,3,5,etc…shown). The x-axis runs top-down (left-right) along the ξ coordinate. The max value ξ (about 4.5) corresponds to SI parameters $T^*$=270K, χ=1 and $\pi_s^*$=1000hPa. These kernels are positive, show vertical spread dependent on the horizontal scale and they are also symmetric in the sense that GF(x,y)=GF(y,x). This last property cannot be captured in this 1-D plot, where the dependency on the first argument of the GF that corresponds to the HIRLAM level is not displayed.*

The different properties of the GF kernels described in the caption of Figure 1 are also those of a covariance matrix. In fact, it is not difficult to establish analogies between this scheme and the standard 3D-Var that clearly suggest that it is possible to think of the GF as a covariance function for the vertical velocity [9].

# 3 Tests of the Variational Constraints Method

## 3.1 Tests with Synthetic Observations

Two HARMONIE-AROME runs are prepared for a period of two days (2013/12/05-06) over a domain 800x800xL65 at nominal horizontal resolution of 2.5 Km. The runs setup are identical (defaults v40h1.1) except for the use of boundary conditions. The reference run or "truth" employs ECMWF analysis ("analysis_only" strategy), while the experiment is nested to closest in time ECMWF forecasts ("simulate_operational" strategy). The reference cycles every 6 hours (coincident with availability of ECMWF analyses), and generates forecasts every hour up to six hours, just what is necessary to carry over information from one cycle to the next, while the experiment operates in a similar configuration but with a shorter 1 hour cycle. No data assimilation is done for any run. For the run acting as truth, we pick up the +3H forecast from cycle 2013/12/05 12 UTC (12 hours after beginning of the experiment), and extract a cube 100x100xL[15-55] situated about the (400,400) point. Fields of wind, vertical divergence, temperature, surface pressure and pressure departure are read off the FA file and compared with their counterparts for the 2013/12/05 14 UTC +1H experiment forecast. The differences (ref-exp) provide the experimenter with "d-fields" ($x_o - x_b$) for horizontal divergence, vertical wind, temperature, surface pressure and pressure departure. We can now make use of these fields to study the congruence between analysed increments by the VC method and "true" increments. For instance, we can compare analysed and "ref-exp" vertical wind increments if we input horizontal divergence "ref-exp" increments to the VC algorithm. In other words, to what extent VC is able to reconstruct vertical motions from horizontal divergence information? Other similar tests can be carried out.

The tests are satisfactory albeit some mismatch in magnitude is found. For instance, Figure 2 shows that the analysed vertical velocity increments (contours) are in good agreement with those expected (shaded) when synthetic HD observations are utilised (i.e. in Eq2.10 notation $F^o_{gw} = F^o_T = F^o_\pi = 0$, $F^o_{HD}$= (ref-exp) ). The plot on the left is for w=1 and that on the right w=10. The bigger the value of w, the tighter the fit to obs as expected. However, the plot on the left also indicates that the analysed w fields come out about one order of magnitude smaller than expected. Due to linearity, is not difficult to introduce an overall scale in the scheme that achieves an impressive match between actual and expected results (plot on the right includes this scale correction). However, this "fine-tuning" resource might not give in practice better verification scores (preliminary results in fact point in this direction). The method should be able to "nudge" towards the right magnitude by frequent updates. One question naturally arises here, is this disparity due to the rather different numerics employed in the VC analysis and in the forecast?

Figure 3 shows on the left the correspondence between horizontal divergence and vertical divergence for analysed fields. On the right, the counterpart for the reference is displayed. This reference is obtained by plotting the VD and HD fields from a +3H forecast. The almost exact out-of-phase relation between these two fields is striking. The analysed fields clearly keep this balance!

Figure 4 illustrates which is the situation for pressure departure PD. This field is analysed from the vertical momentum equation and indeed there is a clear connection between PD and vertical velocity W. However, again a mismatch in magnitude between analysed PD increments and those expected (shaded) is apparent. The mismatch is about one order of magnitude, analysed fields now bigger than

reference. Also the analysed PD lacks some fine scale features. This may be due to how the vertical momentum equation is integrated. Again, also the different numerics employed may be responsible for this mismatch.

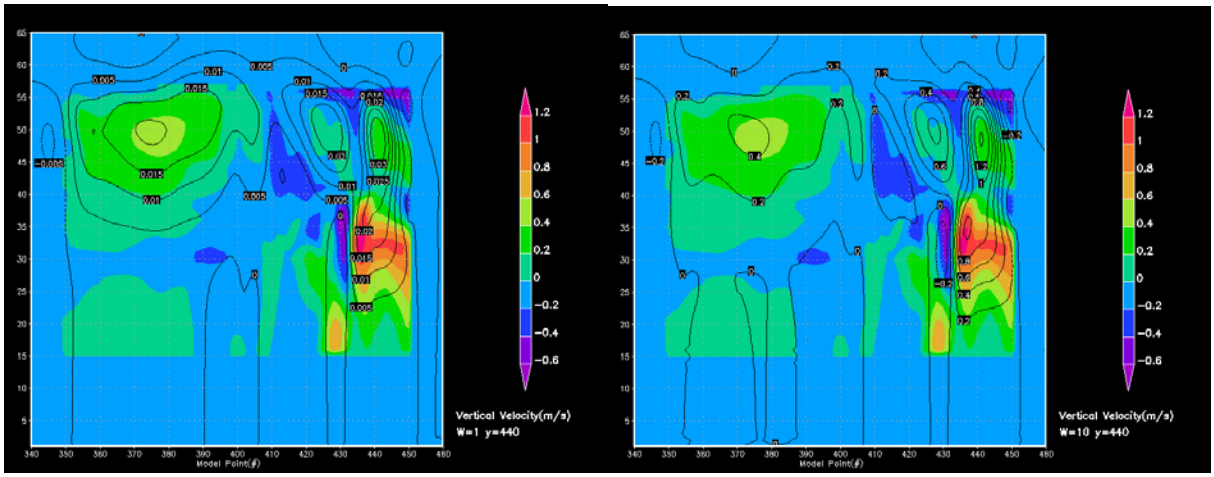


***Figure 2*** *Analysed vertical velocity W from horizontal divergence data HD by means of VC. Left w=1, contours are about $10^{-1}$smaller than shaded values (colour scale on plot). Right w=10, contours capture more structure from the shaded field. The plot on the right includes an overall scale correction which makes agreement between "exp" and "ref" truly remarkable.*

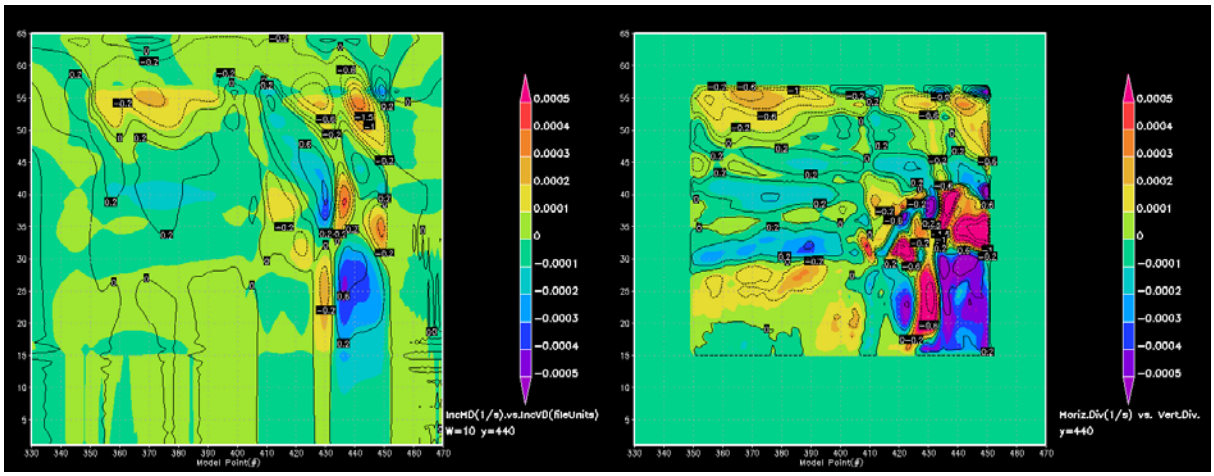


***Figure 3*** *Analysed fields of VD and HD (left) keep the out-of-phase relation that these fields have in mature forecasts (right). Shaded is for HD and contour for VD in both plots.*

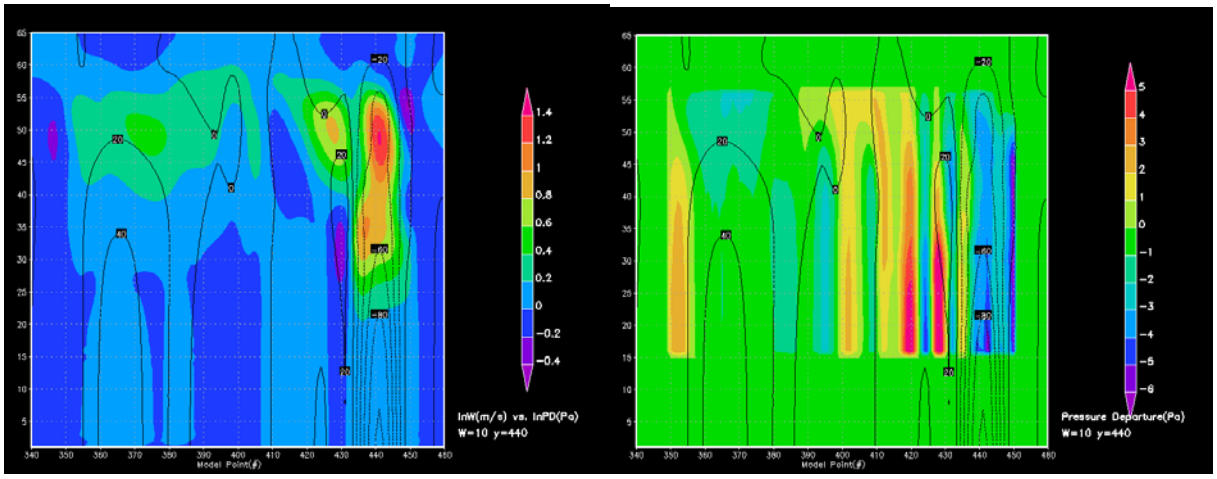


***Figure 4*** *On the left an example of Analysed PD (contour) and W fields (shaded). The pattern shows a clear connection between both, as dictated by the vertical momentum equation. On the right the same PD field displayed on the shaded PD reference. Qualitative agreement is good, but there is a mismatch in magnitude of about one order of magnitude, with analysed PD bigger than reference PD.*

### 3.2 Tests with Model Fields Aligned with Radar Pseudo-Images

If we add a third HARMONIE-AROME run to the previous set of simulations, identical in configuration to the 1-hour cycle run, but with the only difference that we assimilate in this new run Doppler Wind (DOW) radar pseudo-images by means of the field-alignment (FA) technique, we obtain a dataset that can be used to check the impact of assimilating these pseudo-images on short-range HARMONIE-AROME forecasts. We can call these three simulations NAT, TW0 and TW1 respectively. The procedure goes then as follows. From NAT we produce radar pseudo-images of reflectivity and DOW, although only the last ones will be used. The location and scan elevations correspond to a fictitious radar at 400,400 with two elevations at 0.5 and 1.5. We utilize these images to correct +1H forecasts in TW1 for 20 consecutive hourly cycles (2013/12/05 15UTC – 2013/12/06 23 UTC). We also use these pseudo-images as verification data for +1H forecasts by computing DOW differences (NAT-TW0) and (NAT-TW1) for that period.

The FA technique and some experiments with it have been presented elsewhere [11]. The alignment process generates imbalances that can be ameliorated if they are “up-scaled” with the covariance matrix B [11]. In this new test, the up-scaling is substituted by the VC method. Figure 5 (left) shows, somewhat disappointingly, that most of the impact is gone by the first hour. This could be due to FA corrections moving fast out of the radar range and therefore not showing up in the verification. In fact, the area chosen was swept by very strong winds (about 30-40 m/s) during most of the experiment period. In the figure one can indeed identify a dependency of the impact with mean error magnitude (first cases of the series show better impact). Also, it turns out that VC is by itself not able to spread increments significantly in the horizontal (Figure 5 right). VC is mostly about vertical dynamics and balances. It is expected that further enhancements of the algorithm to deal with this problem will improve its performance.

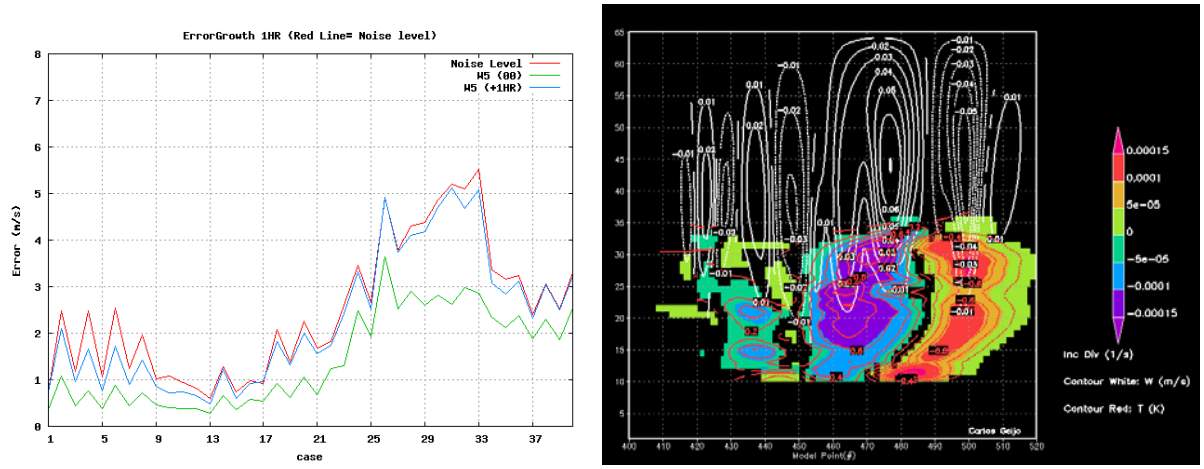


***Figure 5*** *On the left, the impact on 1H forecasts of assimilating DOW data by FA technique, plus additional balancing with the VC method (w=5) is shown. The green curve corresponds to* $(NAT\text{-}TW1)_0$ *for all the cases included in the experiment. This parameter is DOW averaged for each elevation. As two elevations are considered, the total number of cases is 20x2.The blue curve is* $(NAT\text{-}TW1)_{+1}$ *and the red curve is (NAT-TW0) for the same time (i.e. null impact). When the blue curve reaches the red one, the impact has either dissipated or moved away of the radar range. On the right, a vertical cut showing the balanced increments of horizontal divergence (shaded), vertical velocity (white contours) and T (red contours).*

### 3.3 VC as filter for LETKF Analyses

The Local Ensemble Transform Kalman Filter (LETKF) is an efficient ensemble-based variant of the Kalman Filter algorithm [7]. As pointed out in [7], localization may imply the need for some balancing before using these analyses as initial conditions. The goal of this test is to check whether VC can be used in an effective way for this task. A small 10 member ensemble generated by the SLAF method is used to run a 3H assimilation cycle LETKF experiment during a period of ten days (2012/09/20-2012/09/30). The domain is 576 x 480 x L65 big at a nominal horizontal resolution of 2.5Km. Only conventional in-situ observations were utilized (~$10^3$ obs/cycle). As the focus is on upper-air analyses, no surface data assimilation was done. To measure the impact on balance in the first hours of the forecast, a surface pressure tendency metric was used. Standard verification of mean-ensemble forecast and ensemble RMSE and Spread for lead times up to 12H were also carried out.

First we compare the surface pressure tendency evolution for a forecast initialized with the mean LETKF analysis $x^a$, and that initialized with this same analysis filtered as follows

$$(x^a)^* = x^b + VC\,[\,x^a - x^b\,] \qquad \text{Eq 3.3.1}$$

Where the second term on the r.h.s denotes the application of the VC scheme to the (mean) analysis increments. In the notation of Eq2.10, we then have $F^o_D$ , $F^o_T$ , $F^o_\pi$ given by LETKF (mean) increments and $F^o_w = 0$ (as our LETKF does not consider analysis of vertical velocity). In Figure 6 the result of this test is shown. The difference between the green and red lines indicates that indeed in this case localization has produced imbalances. The red line corresponds to an integration started from a 3H forecast and it marks the “0-noise” situation. The thin blue, purple and cyan lines correspond to runs initiated from filtered analysis with VC for three different w parameter values, 10, 5 and 1 respectively, that is, with increasing weight for the variational constraints. The case w=1 achieves reasonably good performance, while the other two cases show poor results. This problem has been traced down to the analysis of pressure departure (PD) and the issue of mismatch in order of magnitude between forecasted PD fields and VC analysed PD fields mentioned above. In the following results, an ad-hoc PD dumping factor (~1/10) has been used to minimize these oscillations in pressure tendency for big values of w.

With respect to forecast verification, the skill of the mean forecast is equivalent with and without VC as far as the standard verification method can tell (not shown). Also in the standard verification of the mean forecast, there was no evidence that the scaled version of VC gives better scores than the no scaled version (not shown). To assess the impact on ensemble RMSE and Spread, an experiment with VC filter applied to all ensemble members was conducted and the results compared to those obtained with a non-filtered ensemble or "raw" ensemble.

$$(x^{a(i)})^* = x^b + VC\,[\,x^{a(i)} - x^b\,] \quad i=1,2,\ldots,10$$

As one would expect, in general the filtered ensemble has less spread, but this decrease in spread does not produce worse RMSE scores. Figure 7 picks up two verifications to illustrate this discussion. On the left we have the verification for surface pressure. It is noticeable that the peak in spread for +1H forecast is reduced by VC. The aspect of the curve "spread vs. forecast range" casts doubts about this spread being spurious. It is clear then that VC has in this case been able to filter noise rather than removing genuine uncertainty measure. On the right, the verification for wind speed at 10m is shown. Here the spread vs. lead time curves are smooth but the one for the filtered case shows a clear increase with forecast range, as one would expect if uncertainty builds up as forecast develops in time. This increase is not seen in the "raw" case, where spread remains at a nearly constant value during the whole integration. As mentioned, RMSE scores are indistinguishable. In these experiments it was found that results with w=10 are to be preferred to smaller values of w, if there is much concern with the loss of spread.

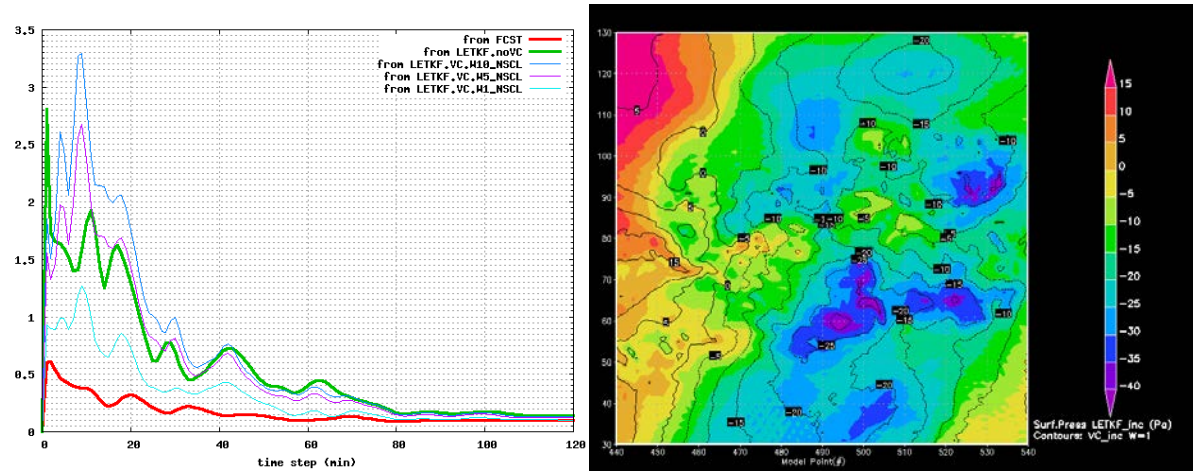


***Figure 6*** *On the left evolution at time step resolution of a surface pressure tendency based metric. The green line corresponds to a run with mean LETKF analysis as IC, the red one is for the same case but with a 3H forecast as IC. Imbalances are present in the LETKF analysis. The thin lines correspond to this LETKF analysis filtered by VC for three different values of w (see text). On the right a snap-shot of the Ps analysis as produced by LETKF (shaded) and after VC filtered (contours).*

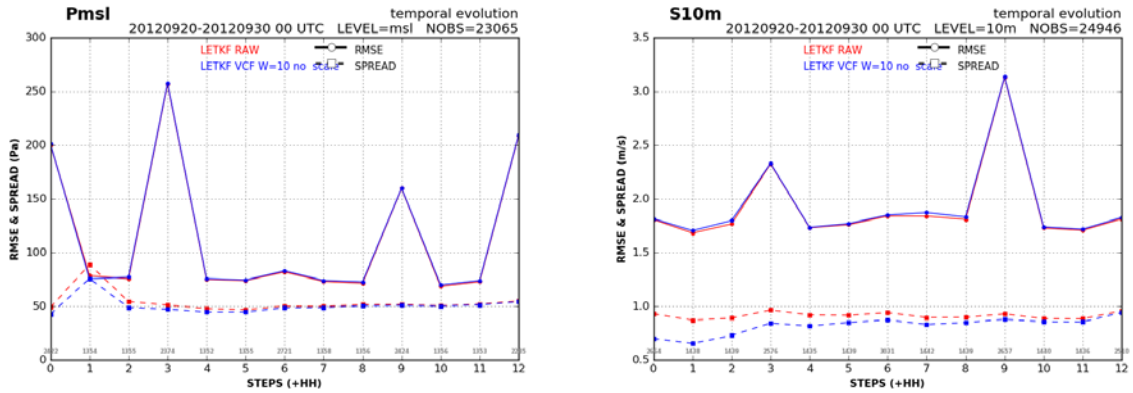


***Figure 7*** *Ensemble RMSE and Spread vs forecast range for the experiment whose settings are presented in the text. Left surface pressure, right wind speed at 10m. See text.*

### 3.4 Comparison between VC and 3D-VAR Statistical Balances

The last test in this first set of investigations on the issue of VC for DA in ALADIN-NH dynamics, aims at comparing the performance of these VC constraints versus the statistical balances encoded in the current 3D-VAR algorithm [8]. To this end, experiments for the same period, domain, assimilation cycle (3H), and observation usage as those employed in the LETKF test were performed. The control now is a standard 3D-VAR, while the experiments consist of univariate 3D-VAR followed by analysis increments filtered by VC to account for inter-dependencies among analysed variables, that is, processed as indicated by Eq 3.3.1 but now with $x^a$ denoting one univariate 3D-VAR analysis instead of one (mean) LETKF analysis. Different values and options for the VC "tunable parameters" were considered (i.e. w weight, scale vs. no scaled, etc…). The following two panels, and the text at the foot, summarize the results obtained in this exercise.

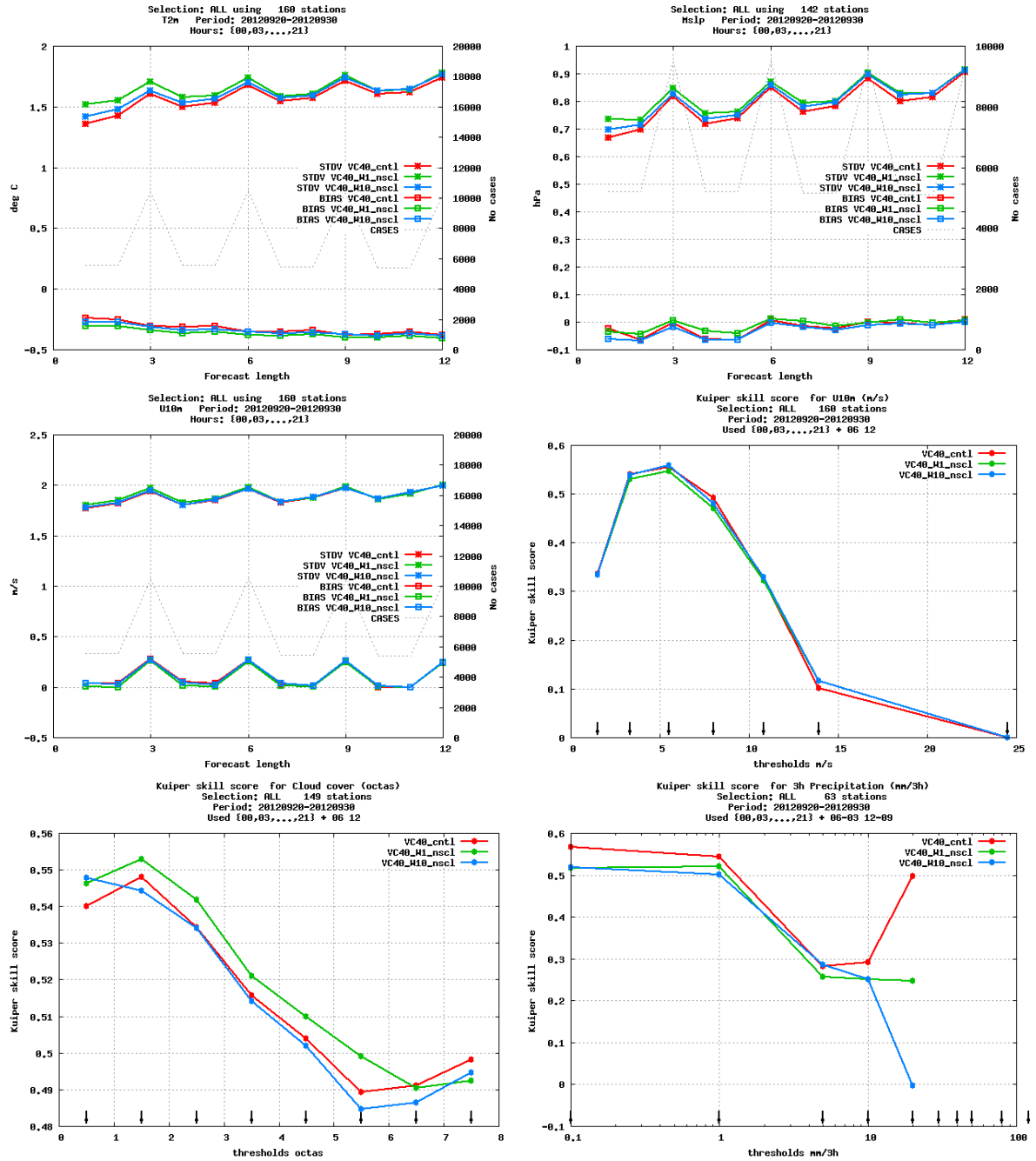


***Figure 8*** *Some verification scores for the VC vs StatBal comparison. This set of plots corresponds to a "**minimal VC tuning**" with all the active w's (i.e. for HD, T and $\pi_s$) equal to 1 (green lines) or 10 (blue lines). The red lines are for CNTL (3D-VAR with StatBal). On the first row we have $T_{2m}$ and mslp. VC degrades these scores, with a tighter fit to increments (w=10) being closer to CNTL. The middle row corresponds to near surface wind (error vs lead time left and Kuiper Skill Score by thresholds to the right). Here the impact can be judged as neutral. The bottom row is for Cloud Cover (Kuiper Skill Score by thresholds) on the left and 3hours precipitation intensity (also Kuiper Skill Score by thresholds) on the right. Most constrained experiment (w=1) gives now somewhat better scores. In all cases the "no-scaled" version is shown. The "scaled" version turns out to give equivalent results (not shown)*

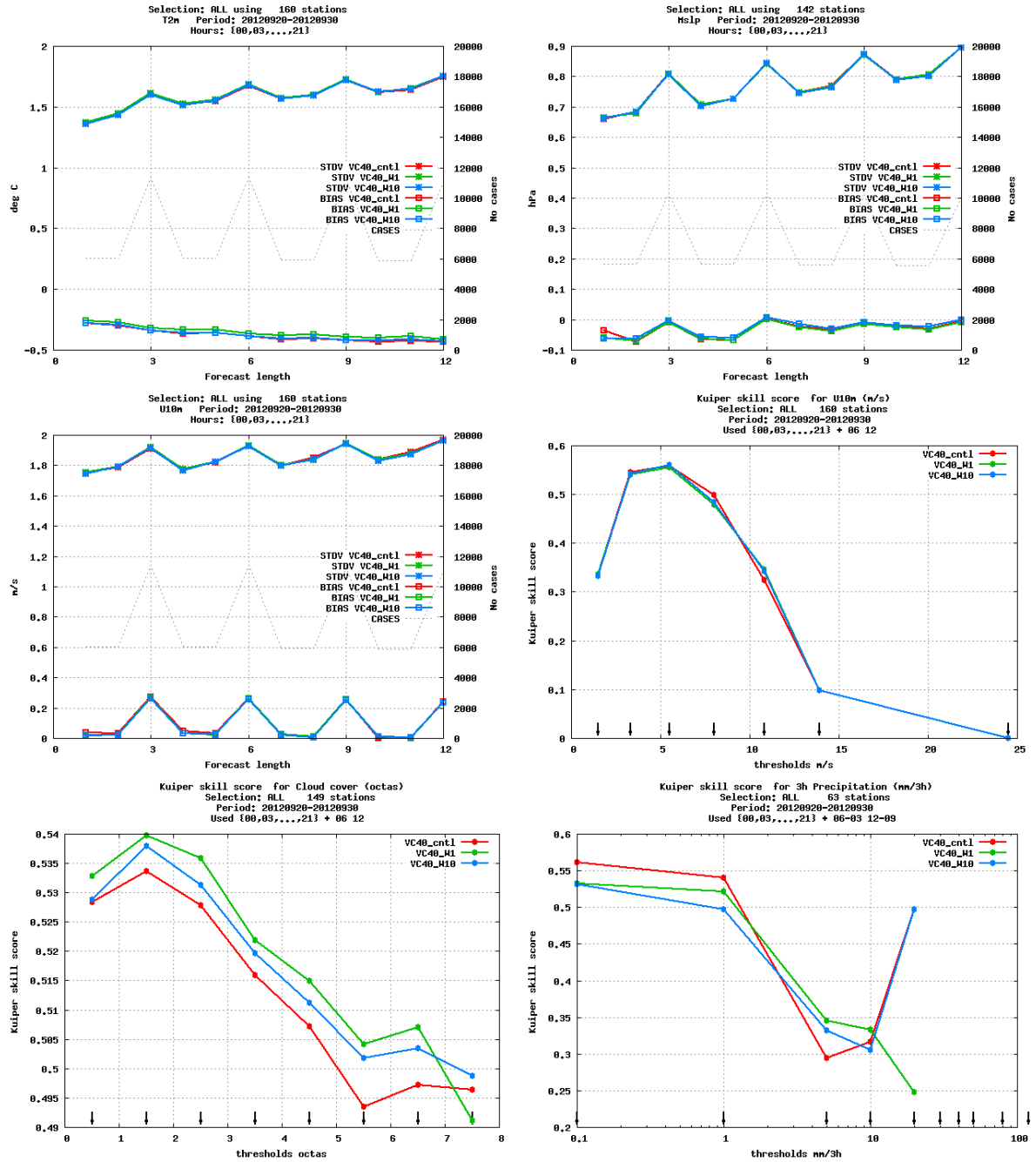


***Figure 9*** *This panel has the same lay out as the previous figure (#8). In this instance the verification scores correspond to "**Fine-tuned VC**", where weights for T and $\pi_s$ are now given a big value (w=100), and w for HD equal to 1 (green lines) or 10 (blue lines). In this experiment, VC was applied to analysis increments with StatBal also incorporated. The red line again corresponds to CNTL (again, 3D-VAR with StatBal). The deterioration in $T_{2m}$ and $\pi_s$ is now gone, and there is virtually no change for near surface wind. The interesting point in this case is the improvement in cloud cover and 3H precipitation intensity, with still the strong constrained case (w=1 vs. w=10) giving the best results. One would like to conclude that this improvement is caused by inclusion of vertical velocity in the analysis.*

# 4 Conclusions

The SI equations define dynamic relations among several variables that can be used in DA. A new algorithm that implements this idea is given by the solution to a variational (weakly) constrained

problem. The solution is obtained using Greens Functions. The SI system is a time-step forward operator, and this property gives to this new algorithm a nudging-like functionality, which makes it well suited for "continuous-in-time" DA. It also brings to the DA process the vertical velocity and PD fields.

A first implementation of this method has demonstrated its capacity to provide good equilibrium among horizontal and vertical momentum analysed fields. However, some mismatch in magnitude between analysed and forecast vertical velocity and PD fields has been observed. This will be the object of more investigation.

The method has also demonstrated its potential to improve vertical balances of assimilated wind fields generated by FA with radar DOW pseudo-images. First results so far can however be surely enhanced with further treatment of the FA increments (horizontal up-scaling).

First experiments with the LETKF DA algorithm (3h DA cycle, only conv-obs) have shown that this algorithm can filter spurious oscillations in the surface pressure tendency field. At difference with other digital filters, the filter design is almost completely dictated by the SI dynamics. On the other hand, standard verification scores show a clear reduction in ensemble spread. Although this result is to be expected, there is no simultaneous reduction in ensemble error and stochastic verification scores in consequence are not completely favourable. Also, first results with 3D-VAR do not show big gains with respect to the statistical balances method. All these tests however, have been done with 3 hours DA cycles and small amount of observations, conditions where initialization issues do not manifest in the foreground. Also the rather different numerical techniques employed in VC analysis and forecasts must clearly bias the results towards the wrong side. The introduction of some ad-hoc tuneable parameters helps to improve the verification scores.

# 5 References

**[1]** Sasaki, Y. "Some Basic Formalisms in Numerical Variational Analysis", Monthly Weather Review, Vol 98, No.12, Dec 1970a, pp 875-883

**[2]** Thompson, P. "Reduction of Analysis Error through Constraints of Dynamical Consistency", Journal of Applied Meteorology, Vol 8, No.5, Oct 1969, pp 738-742

**[3]** Wahba, G. and Wendelberger, J. "Some New Mathematical Methods for Variational Objective Analysis using Splines and Cross Validation", Monthly Weather Review, Vol 108, Aug 1980, pp 1122-1143

**[4]** Fischer, C. et al., 2005 "An Overview of the Variational Assimilation in the ALADIN/France NWP System", Q.J.R. Meteorol. Soc. 131; 3477-3492

**[5]** Geijo, C. , 2015 "A New Solver for the Non-Hydrostatic Semi-Implicit Scheme in HARMONIE using Green Functions", HIRLAM-ALADIN Newsletters #5 pp 138-162. (http://www.umr-cnrm.fr/aladin/IMG/pdf/nl5.pdf) https://www.researchgate.net/publication/281293331_A_new_Solver_for_the_Non-Hydrostatic_Semi-Implicit_Scheme_in_HARMONIE_using_Greens_Functions DOI: 10.13140/RG.2.1.4076.4646

**[6]** Ravela, S. et al, 2007 "Data Assimilation by Field Alignment", Physica D 230, pp 127-145 (available from www.sciencedirect.com ).

**[7]** Hunt B.R. et al, 2007 "Efficient Data Assimilation for Spatiotemporal Chaos: A Local Ensemble Transform Kaman Filter", Physica D 230 pp 112-126 (available from www.sciencedirect.com )

**[8]** Derber J. and Bouttier F. "A Reformulation of the Background Error Covariance in the ECMWF Global Data Assimilation System", Tellus, 51A, 1999, pp 195-221

**[9]** Geijo, C., 2018 "ANNEX to Variational Constraints for Data Assimilation in ALADIN-NH Dynamics". https://www.researchgate.net/publication/326467111_ANNEX_to_Variational_Constraints_for_DA_in_ALADIN-NH_Dynamics. DOI: 10.13140/RG.2.2.17448.06402

**[10]** Bénard, P. et al., 2010 "Dynamical Kernel of the ALADIN-NH Spectral LAM: Revised Formulation and Sensitivity Experiments", Q.J.R Meteorol. Soc. 136, 155-169

**[11]** Geijo, C. 2013, Presentation at the 6th WMO Conference on Data Assimilation. https://www.researchgate.net/publication/281236886_Assimilation_of_Weather_Radar_Data_in_a_Convection_Permitting_NWP_System_using_the_Field_Alignment_Technique.

**[12]** Laprise, R. "The Euler Equations of Motion with Hydrostatic Pressure as an Independent Variable", Monthly Weather Review , Vol 120, January 1992, pp 197-207